ACS Catalysis

Research Article

pubs.acs.org/acscatalysis

Support Induced Control of Surface Composition in Cu−Ni/TiO_2 Catalysts Enables High Yield Co-Conversion of HMF and Furfural to Methylated Furans

Bhogeswararao Seemala,[†,‡] Charles M. Cai,[†,‡] Charles E. Wyman,[†,‡] and Phillip Christopher*[,‡,§,∥]

[†]Bourns College of Engineering - Center for Environmental and Research Technology (CE-CERT), University of California, Riverside, California 92507, United States

[‡]Department of Chemical and Environmental Engineering, Bourns College of Engineering, University of California, Riverside, California 92521, United States

[§]Program in Materials Science, University of California, Riverside, Riverside, California 92521, United States

[∥]UCR Center for Catalysis, University of California, Riverside, Riverside, California 92521, United States

Supporting Information

ABSTRACT: 5-(Hydroxymethyl)furfural (HMF) and furfural (FF) have been identified as valuable biomass-derived fuel precursors suitable for catalytic hydrodeoxygenation (HDO) to produce high octane fuel additives such dimethyl furan (DMF) and methyl furan (MF), respectively. In order to realize economically viable production of DMF and MF from biomass, catalytic processes with high yields, low catalyst costs, and process simplicity are needed. Here, we demonstrate simultaneous coprocessing of HMF and FF over Cu−Ni/TiO_2 catalysts, achieving 87.5% yield of DMF from HMF and 88.5% yield of MF from FF in a one pot reaction. The Cu−Ni/TiO_2 catalyst exhibited improved stability and regeneration compared to Cu/TiO_2 and Cu/Al_2O_3 catalysts for FF HDO, with a ∼7% loss in FF conversion over four sequential recycles, compared to a ∼50% loss in FF conversion for Cu/Al_2O_3 and a ∼30% loss in conversion for Cu/TiO_2. Characterization of the Cu−Ni/TiO_2 catalyst by X-ray photoelectron spectroscopy, scanning transmission electron microscopy, and H_2−temperature-programmed reduction and comparison to monometallic Cu and Ni on Al_2O_3 and TiO_2 and bimetallic Cu−Ni/Al_2O_3 catalysts suggest that the unique reactivity and stability of Cu−Ni/TiO_2 derives from support-induced metal segregation in which Cu is selectively enriched at the catalyst surface, while Ni is enriched at the TiO_2 interface. These results demonstrate that Cu−Ni/TiO_2 catalysts promise to be a system capable of integrating directly with a combined HMF and FF product stream from biomass processing to realize lower cost production of liquid fuels from biomass.

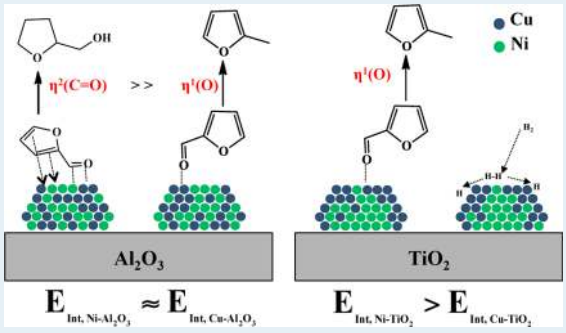

KEYWORDS: *furfural, hydroxymethyl furfural, hydrodeoxygenation, bimetallic catalysts, biofuels, support effects*

1. INTRODUCTION

Lignocellulosic biomass is the most abundant and inexpensive renewable resource that can potentially displace petroleum as a carbon neutral alternative for the production of fungible liquid transportation fuels and commodity chemicals.[1−4] However, the production of target chemicals and gasoline range fuels from lignocellulosic biomass has been economically challenging due to the need for multiple processing steps and associated high product yields required in each step.[5,6] Biomass is rich in both C_6 (glucan) and C_5 (xylan) polymeric sugars that can be converted by acid-catalyzed dehydration into 5-(hydroxymethyl)furfural (HMF) and furfural (FF), respectively, with high yields.[7−11] As such, HMF and FF have been identified as valuable fuel precursors suitable for the production of dimethyl furan (DMF) and methyl furan (MF), respectively, through selective hydrodeoxygenation (HDO) (hydrogenation followed by hydrogenolysis). Due to their high octane numbers, these methylated furans (DMF and MF) have been deemed as valuable target fuel products from biomass suitable for blending with gasoline.[12] DMF and MF can also be selectively converted into C_6 and C_5 alcohols as direct gasoline replacements or further converted into long chain hydrocarbons for diesel or jet fuel applications by condensation followed by deoxygenation.[13,14] However, catalytic production of DMF and MF from biomass derived HMF and FF requires high yields and process simplicity.

Supported noble metal catalysts have been thoroughly studied for HDO of HMF and FF. To reduce costs and control toxicity from catalyst wastes, heterogeneous base metal catalysts, particularly first row transition metals such as Ni, Cu,

Received: April 3, 2017
Revised: May 2, 2017
Published: May 8, 2017

DOI: 10.1021/acscatal.7b01095
ACS Catal. 2017, 7, 4070−4082

Co, and Fe, are excellent choices.[15−17] Undesired reactions such as decarbonylation and ring hydrogenation are common when using base metal catalysts (particularly Ni, Co, and Fe), and the stability of these materials under reaction conditions is low at high temperatures (≥200 °C).[18−20] FF conversion to MF occurs through hydrogenation to furfuryl alcohol (FOL) as an intermediate product, followed by hydrogenolysis to MF.[21,22] Unwanted side reactions include ring hydrogenation of MF or FOL to form methyl tetrahydrofuran (MTHF), or tetrahydrofurfural alcohol (THFOL) and decarbonylation of FF to form furan, see Scheme 1. Cu catalysts minimize

Scheme 1. Reaction Pathway for FF Conversion[a]

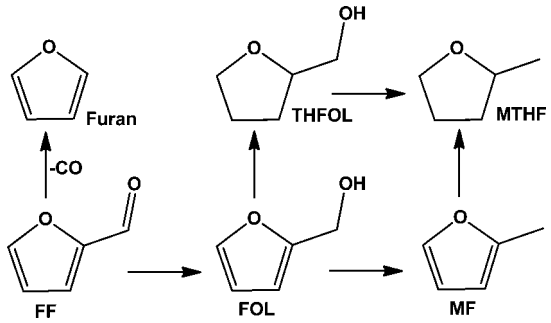

[a]FF = furfural, FOL = furfuryl alcohol, MF = methyl furan, THFOL = tetrahydrofurfuryl alcohol, and MTHF = methyl tetrahydrofuran.[22]

decarbonylation and ring hydrogenation due to their full valence d-band and effectively hydrogenate FF to FOL at low temperatures (<200 °C).[23−26] However, the low activity of Cu for H_2 activation and stronger interaction of Cu with FF, as compared to FOL, make conversion of FOL to MF on pure Cu catalysts slow.[27−29] Cu-based bimetallic catalysts have been proposed to overcome the low reactivity of monometallic Cu for hydrogenation reactions. Various formulations have been proposed, such as Cu−Fe, Cu−Pd, Cu−Cr, and Cu−Ni,[26,28,30−34] to increase reactivity or selectivity, but further enhancements in reactivity, selectivity toward MF, and catalyst stability are needed for economical implementation.[35]

HMF conversion to DMF is known to occur through hydrogenation and hydrogenolysis of the alcohol and carbonyl groups, but undesirable products are formed through decarbonylation and ring hydrogenation reactions, see Scheme 2. Noble metal catalysts such as Ru, Pt, and Pd and their combination with Cu, Fe, and Co in bimetallic catalysts have been reported for HMF conversion to DMF, although the requirement of Pt group metal catalysts is economically challenging for an industrial process.[36−41] Limited reports exist on the successful use of solely first row transitions metals or non-noble metal catalyst systems for high yield conversion of HMF to DMF.[42] Recently, it has been demonstrated that modifying Cu catalysts with Zn or Co and graphene enabled high selectivity for DMF production.[43] However, in these reports, low reactivity[43] and stability,[42] or expensive catalyst formulations (graphene),[43] limit their commercial viability. Bifunctional Ni catalysts combining dispersed Ni species and acidic supports have also been demonstrated for HMF conversion to DMF with high yields, although these reports are limited by catalyst stability[44] or require high H_2 pressures.[45]

It is clear that base metal catalysts are most suitable for HDO of FF and HMF to methyl furans due to their low costs, but limited demonstrations of these catalysts are reported to achieve high reactivity, selectivity, and stability. Furthermore, it has recently been demonstrated that high yield coproduction of HMF and FF can be achieved directly from biomass in a single step process using THF as a cosolvent, thereby enabling integrated downstream catalytic strategies to process a single product stream containing both HMF and FF to reduce overall processing costs.[11] However, most previous reports on HMF and FF HDO have considered their catalytic conversion separately. It is expected that coupling base metal catalysts capable of simultaneously converting HMF and FF to methylated furans with recently developed biomass pretreatment technologies could realize significant cost savings for an integrated processing strategy that avoids separating biomass sugar streams.

Here, we demonstrate ∼90% yields, high reactivity, good stability, and regenerative behavior for TiO_2 supported Cu−Ni bimetallic catalysts in individuals and coprocessing of FF and HMF to MF and DMF, respectively. Detailed characterization and reactivity comparison of monometallic Cu and Ni and bimetallic Cu−Ni supported on TiO_2 and Al_2O_3 demonstrate that for Cu−Ni/TiO_2, core−shell structures form in which Cu is enriched at the catalyst surface. It is proposed that this structure forms due to strong and preferential interactions between Ni and TiO_2 that reduce the concentration of Ni at the catalyst surface, thereby allowing Ni to promote Cu reactivity without compromising selectivity. It is expected that the use of metal−support interactions to control the exposed metal composition in bimetallic catalysts should be generally useful for enhancing selectivity, reactivity, and stability in a variety of catalytic processes.

2. MATERIALS AND METHODS

2.1. Synthesis of Monometallic Cu and Ni Catalysts. In a typical synthesis, copper(II) nitrate trihydrate ($Cu(NO_3)_2 \cdot 3H_2O$, Aldrich, purity 99%, CAS: 10031-43-3, New Jersey,

Scheme 2. Reaction Pathway for HDO of HMF to DMF[a]

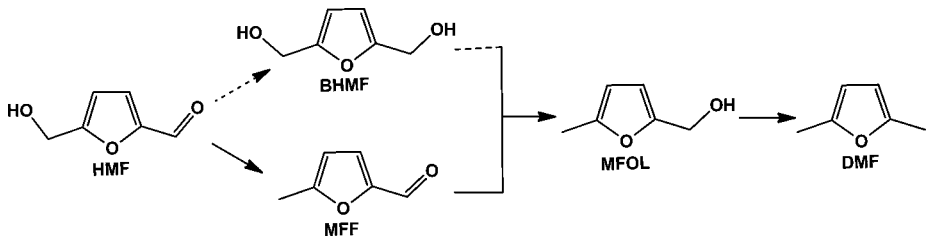

[a]HMF = 5-hydroxymethyl furfural, MFF = methyl furfural, BHMF = bis(hydroxymethyl) furan, MFOL = methyl furfuryl alcohol, and DMF = dimethyl furan.[2]

DOI: 10.1021/acscatal.7b01095
ACS Catal. 2017, 7, 4070−4082

USA) was dissolved in 50 mL of deionized (DI) water and added to 5 g of θ-Al_2O_3 (Inframat Advanced Materials, Catalogue no: 26R-0804UPG, Manchester CT 06042, USA) or TiO_2 (P25, NIPPON AEROSIL Co., LTD, Evonik, Degussa GmbH, Batch No. 4161060398) contained in a round-bottom flask to obtain a 10 wt % loading of Cu. The solution was mixed and dried at 80 °C in a rotary evaporator. Supported Ni catalysts were prepared similarly to Cu catalysts, where nickel(II) nitrate hexahydrate ($Ni(NO_3)_2{\cdot}6H_2O$, Aldrich, purity 99.99%, Louis, MO 63103, USA) was used as a precursor in desired quantities to achieve 10 wt % loadings on TiO_2 and θ-Al_2O_3. The resulting solids were dried at 100 °C for 12 h in an oven and calcined at 450 °C for 5 h. Prior to reactivity experiments, catalysts were reduced by a pure H_2 flow rate of 50 mL min^{-1} at 450 °C for 3 h and cooled to 25 °C under the same environment.

2.2. Synthesis of Bimetallic Cu−Ni Catalysts. Required amounts of Ni and Cu precursors to achieve 5 wt % loadings of each metal were mixed simultaneously in 50 mL of DI water and added to 5 g of TiO_2 or θ-Al_2O_3 in a round-bottom flask. These materials were then mixed and dried at 80 °C in a rotary evaporator. The solid was collected and dried at 100 °C for 12 h in an oven followed by calcining at 450 °C for 5 h. Prior to reactivity experiments, catalysts were reduced by pure H_2 at a flow rate of 50 mL min^{-1} at 450 °C for 3 h and cooled to 25 °C under the same environment.

2.3. Catalyst Characterization Techniques. *2.3.1. X-ray Diffraction (XRD).* XRD spectra of reduced catalysts were recorded in the 2θ range of 20 to 90° using an X'pert Pro PANalytical diffractometer equipped with a Nickel filtered Cu Kα radiation source.

2.3.2. Surface Area. The total accessible surface area (S_{BET}) of the catalysts was measured by N_2 physisorption using a Micromeritics ASAP 2020 instrument.

2.3.3. Scanning Transmission Electrom Microscopy (STEM). STEM imaging was performed at 300 kV accelerating voltage on an FEI Titan Themis 300 instrument fitted with an X-FEG electron source, a three lens condenser system, and an S-Twin objective lens. STEM images were recorded with a Fischione Instruments Inc. M3000 High Angle Annular Dark Field (HAADF) Detector at a probe current of 0.2 nA, frame size of 2048 × 2048, dwell time of 15 μs/pixel, camera length of 195 mm, and convergence angle of 10 mrad. Elemental X-ray microanalysis and mapping were performed utilizing an FEI Super-X EDS system with four symmetrically positioned SDD detectors of 30 mm^2 each, resulting in an effective collection angle of 0.7 srad. Elemental maps were collected in STEM mode with a beam current of 0.4 to 0.25 nA with a 512 × 512 pixel frame, dwell time of 30 μs, and acquisition time of up to 10 min. Specimens prepared from suspension in distilled water were deposited on copper grids coated with a lacey carbon. Average metal particle sizes were measured based on the diameter of 100 particles from corresponding TEM images of each catalyst.

2.3.4. X-ray Photoelectron Spectroscopy (XPS). XPS characterization was carried out using a Kratos AXIS ULTRADLD XPS system equipped with an Al Kα monochromated X-ray source and a 165 mm mean radius electron energy hemispherical analyzer. Vacuum pressure was kept below 3 × 10^{-9} Torr during analysis. Binding energy calibrations were done with reference to the carbon 1s peak by adjusting spectra to 284.8 eV. Depth profiling experiments were conducted by argon sputtering samples for 0, 1, 5, 10, 30, and 60 min with a beam voltage of 4 kV, current of 2.35 A, spot size of 3 × 3 mm^2, and vacuum pressure of 3 × 10^{-9} Torr during acquisition. XPS peak fitting for Cu and Ni components was optimized for each support, and parameters of the fit were kept constant. A fwhm of 2 eV (2.15 eV) and a Gaussian/Lorenzian line shape ratio of 30% (60%) was used for all Cu and Ni peak fitting on Al_2O_3 (TiO_2). The surface composition of bimetallic Cu/Ni catalysts was calculated using sensitivity factors of 5.321 and 4.044 for Cu and Ni, respectively.

2.3.5. Temperature-Programmed Reduction (TPR). TPR experiments were carried out on a Micromeritics AutoChem 2920 instrument. In each experiment, 0.1 g of catalyst was placed in a quartz tube and treated with pure Ar flowing at 30 mL min^{-1} at 150 °C for 1 h. A gas mixture of H_2 (10%)−Ar (90%) was passed through the quartz reactor at 25 °C for 1 h with a 50 mL min^{-1} flow rate. The temperature was raised to 800 °C at a linear heating rate of 5 °C min^{-1}. A standard CuO powder was used to calibrate H_2 consumption.

2.4. Reactivity Measurements. Prior to each reaction, Ni, Cu, and Cu−Ni catalysts were reduced at 450 °C for 3 h. Without exposure to air, 0.3 g of reduced catalysts was transferred into a 100 mL stainless-steel Parr micro benchtop reactor containing 1 g of FF (Sigma-Aldrich, 99.9% pure) with 25 mL of either isopropyl alcohol (Fischer Chemical, HPLC grade) or 1,4-dioxane (Fisher Chemicals, HPLC grade) as a solvent. The reactor was initially flushed with H_2 and then pressurized under pure H_2 environments. Next, the reactor temperature was raised to 25−240 °C, and the reaction was conducted for 1−8 h. An identical protocol was used for the HMF and FF/HMF coprocessing reactions, except in HMF conversion reactions, 0.5 g of HMF was used as a reactant, and for FF/HMF coprocessing reactions, 0.5 g of FF and 0.25 g of HMF were used.

2.5. Product Analysis. Liquid products were analyzed by gas chromatography (Agilent Technologies 7890A; column: DB-WAX Ultra Inert, 30 m long × 0.320 mm internal diameter × 0.5 μm) via FID according to the following program: hold for 1 min at 30 °C; increase from 30 to 100 °C at a ramp rate of 10 °C min^{-1}; 2 min hold at 100 °C; increase from 100 to 250 °C at a ramp rate of 25 °C/min; 0 min hold; increase from 250 to 325 °C at a ramp rate of 25 °C min^{-1}; and 1 min hold at 325 °C. Mass yields of the final product were quantified by using calibration curves of standard samples in the gas chromatograph. Mass balances accounting for >95% of the carbon content were obtained in all experiments. Reactant conversion and product yield were calculated as follows:

$$\text{HMF (or) FF conversion \%} = \left(1 - \frac{\text{moles of unreacted FF}}{\text{moles of FF before reaction}}\right) \times 100$$

$$\text{Yield} = \frac{\text{moles of the product produced}}{\text{moles of HMF (or) FF before reaction}} \times 100$$

2.6. Catalyst Recyclability. A total of 0.3 g of freshly reduced catalysts was transferred into a 100 mL stainless-steel Parr reactor containing 1 g of FF and 25 mL of 1,4-dioxane. The reactor was pressurized with H_2 to 25 bar, and the reaction was conducted for 2 h at 200 °C. The reactor was cooled by quickly lowering it into a room temperature water bath (25 °C) and then depressurized. The catalyst was separated by filtration, dried at 100 °C for 3 h, and then reused in four recycle experiments without reduction or reactivation. Regeneration

DOI: 10.1021/acscatal.7b01095
ACS Catal. 2017, 7, 4070−4082

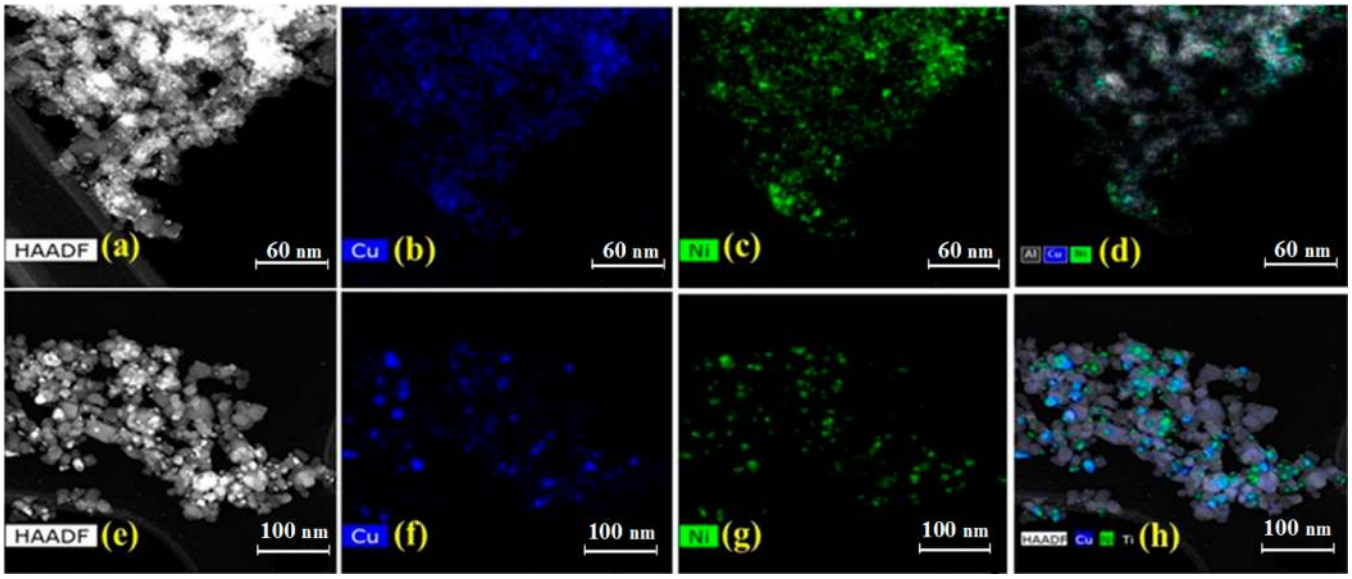

Figure 1. (a) Representative STEM image of the Cu−Ni/Al_2O_3 catalyst and associated (b) Cu, (c) Ni, and (d) overlaid Cu/Ni/Al elemental mapping. (e) Representative STEM image of the Cu−Ni/TiO_2 catalyst and associated (f) Cu, (g) Ni, and (h) overlaid Cu/Ni/Ti elemental mapping.

Table 1. Physicochemical Properties of Monometallic Cu, Ni, and Bimetallic Cu−Ni Catalysts Supported on Al_2O_3 and TiO_2

				Cu/Ni surface composition		
sample	specific surface area (S_{BET}, m^2/g)	particle size distribution from TEM (nm)	H_2-uptake (TPR; mmol/g)	Cu^{2+}/Cu^0	Ni^{2+}/Ni^0	Cu/Ni (Cu^0 + Cu^{2+})/(Ni^0 + Ni^{+2})
θ-Al_2O_3	79.7					
TiO_2 (P25)	54.3					
Cu (10 wt %)/Al_2O_3	64.0	7.0 ± 1.6	1.29	37.6/62.4		
Cu (10 wt %)/TiO_2	43.4	8.0 ± 3.5	1.48	47.8/52.2		
Ni (10 wt %)/Al_2O_3	64.8	6.4 ± 5.1	1.68		52.4/47.7	
Ni (10 wt %)/TiO_2	47.2	9.9 ± 2.6	1.75		57.5/42.7	
Cu (5 wt %)−Ni (5 wt %)/Al_2O_3	67.4	4.9 ± 1.6	1.62	38.6/61.4	73.7/26.3	48.7/51.3[b]
Cu (5 wt %)−Ni(5 wt %)/TiO_2	45.9	7.5 ± 3.9	1.56	33.1/66.9	57.5/42.5	82.4/17.6[b]
Cu (5 wt %)−Ni (5 wt %)/Al_2O_3[a]						47.2/52.8
Cu (5 wt %)−Ni (5 wt %)/TiO_2[a]						82.4/17.6

[a]Catalysts were calcined prior to analysis. [b]Cu/Ni ratio is from XPS shown in Figure 2, and these are consistent with the values in Figure 3.

was executed via calcination at 450 °C for 5 h followed by reduction with pure H_2 at 450 °C for 3 h.

3. RESULTS

3.1. Catalyst Characterization. To explore the influence of support and the formation of bimetallic particles on HDO performance, monometallic Cu (10% weight loading) and Ni (10% weight loading) catalysts and bimetallic Cu−Ni catalysts (5% Cu−5% Ni weight loading) on TiO_2 and θ-Al_2O_3 were synthesized via an impregnation approach. XRD spectra of reduced monometallic (Cu and Ni) and bimetallic (Cu−Ni) catalysts are shown in Figure S1. Reduced monometallic Cu catalysts showed distinct peaks at 43.3° and 50.4° that correspond to the (111) and (200) reflections of metallic Cu, respectively. The reduced monometallic Ni catalysts exhibited clear peaks associated with the (111) reflection of metallic Ni at 44.9°, although in the case of the Ni/Al_2O_3 catalyst this peak overlapped with Al_2O_3 reflections. The Cu−Ni/Al_2O_3 catalyst exhibited a diffraction peak at 43.9°, and the Cu−Ni/TiO_2 catalyst exhibited a diffraction peak at 44.1° and a shoulder at 44.6°. The existence of diffraction peaks between the Cu (111) and Ni (111) reflections for the bimetallic catalysts are evidence of the formation of Cu−Ni alloy phases.[46,47] However, we refrain from using these peak positions to draw conclusions about the nature of the Cu−Ni alloy, as the diffraction peaks are predominantly derived from the largest particles in each catalyst and are not representative of the composition of all particles in each sample.

Representative TEM images of the monometallic and bimetallic catalysts are shown in Figure 1a,b and Figure S2, with corresponding particle size distributions shown in Figure S3 and average particle sizes reported in Table 1. The average metallic particle diameter in all catalysts was relatively consistent, with values between 4.9 and 9.9 nm. It was observed that for a given metal composition, the Al_2O_3 supported catalysts exhibited a ∼1−2 nm smaller average particle diameter compared to the TiO_2 supported catalysts. This is likely due to the ∼20 m^2/g greater total surface area of

DOI: 10.1021/acscatal.7b01095
ACS Catal. 2017, 7, 4070−4082

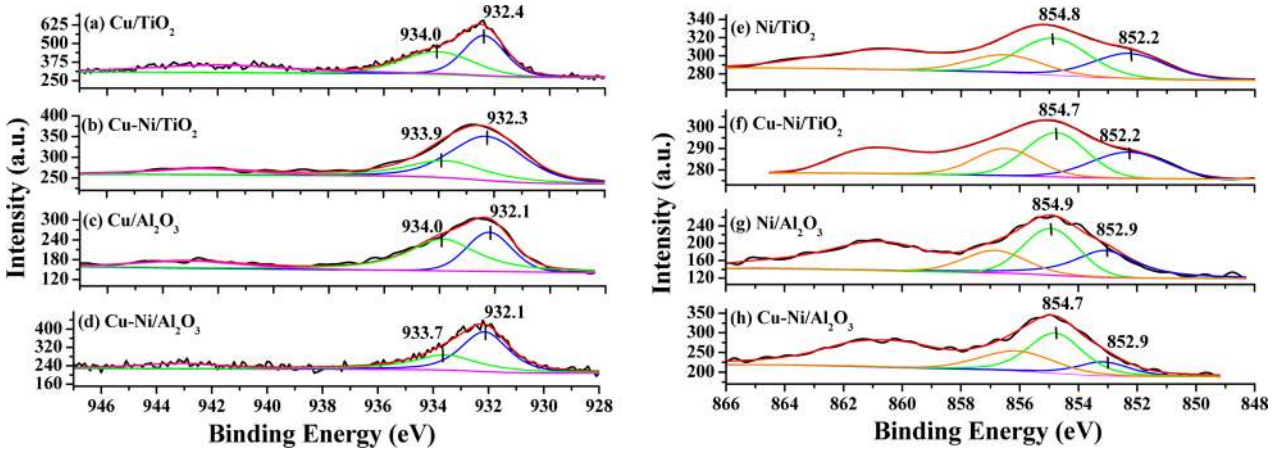

Figure 2. XPS spectra of monometallic and bimetallic catalysts in the Cu 2p3/2 energy window for (a) Cu/TiO_2, (b) $Cu–Ni/TiO_2$, (c) Cu/Al_2O_3, and (d) $Cu–Ni/Al_2O_3$, and in the Ni 2p3/2 energy window for (e) Ni/TiO_2, (f) $Cu–Ni/TiO_2$, (g) Ni/Al_2O_3, and (h) $Cu–Ni/Al_2O_3$. Metallic peaks (Cu^0 and Ni^0) represented with blue color and metal oxide peaks (CuO and NiO) represented with green color. Orange color represents Ni(OH)x peak.

the Al_2O_3 supported catalysts compared to the TiO_2 supported catalysts, see Table 1. From the TEM analysis, we conclude that the active metal particle sizes in all catalysts are relatively consistent, and significant differences in catalyst performance as a function of support for a given metal composition are not expected to be derived from particle size effects. Elemental mapping executed for the $Cu–Ni/TiO_2$ and $Cu–Ni/Al_2O_3$ catalysts shown in Figure 2b–d and f–h demonstrated that Cu and Ni signals coexisted for all observed metal particles. This is consistent with the XRD results, providing evidence that bimetallic Cu–Ni particles formed on both Al_2O_3 and TiO_2.

XPS was used to characterize the oxidation state and surface composition of the monometallic and bimetallic catalysts by analyzing the Cu and Ni 2p3/2 peaks. Because these experiments were performed *ex situ*, the exposure to air when catalysts were transferred from the reduction reactor to the XPS chamber caused partial metal oxidation. Figure 2a–d shows the Cu 2p3/2 spectra for prereduced monometallic Cu and bimetallic Cu–Ni catalysts on Al_2O_3 and TiO_2. All reduced Cu containing catalysts show signatures of Cu^0 with binding energies of 932.1–932.4 eV and Cu^{2+} with binding energies of 933.7–934.0, and the associated shakeup satellite peak at ~943 eV, consistent with the literature.[48] We note that the Cu^+ peak was not included in this analysis due to overlap with the position of the Cu^0 peak, although this is not expected to significantly influence our conclusions.[49,50] Comparing the monometallic Cu catalysts on TiO_2 and Al_2O_3, we observed that the relative fraction of Cu^0 species, with respect to Cu^{2+}, is lower on TiO_2 (52.2% for TiO_2 versus 62.4% for Al_2O_3, Table 1) and that the binding energy of Cu^0 is shifted down from 932.4 eV for TiO_2 to 932.1 eV for Al_2O_3. The increased fraction of oxidized Cu^{2+} and the shift in energy of the Cu^0 peak on the TiO_2 support were likely caused by Cu^0 catalyzed reduction of TiO_2, with subsequent formation of CuO_x species and charge transfer from Cu^0 to CuO_x or TiO_2.[48,51] For $Cu–Ni/TiO_2$, the relative fraction of Cu^0 compared to Cu^{2+} increased to values consistent with those observed for Cu/Al_2O_3 and $Cu–Ni/Al_2O_3$, and the binding energy of the Cu^0 species also shifted down slightly, suggesting weaker interactions between Cu and TiO_2 in $Cu–Ni/TiO_2$ compared to Cu/TiO_2.

In Figure 2e–h, the Ni 2p3/2 XPS spectra are shown for monometallic Ni and bimetallic Cu–Ni supported on Al_2O_3 and TiO_2. All supported Ni catalysts showed three peaks between 852.2 and 853.0 eV, 854.5 and 854.8 eV, and 856.2 and 856.6 eV that are assigned to metallic Ni^0, NiO, and $Ni(OH)_2$, respectively.[52] Binding energies for the Ni^0 2p3/2 peaks were in the order $Ni–Cu/Al_2O_3 \approx Ni/Al_2O_3 > Ni/TiO_2 \approx Ni–Cu/TiO_2$, with the well-known strong interactions between Ni and TiO_2 driving charge transfer from Ti^{3+} to Ni d-states.[53] The shift in binding energy of the Ni^0 2p3/2 peak when comparing the monometallic Ni catalysts on Al_2O_3 and TiO_2 was more significant than that observed for the Cu^0 2p3/2 peak in the monometallic Cu catalysts (0.7 eV versus 0.3 eV), demonstrating stronger interactions and increased charge transfer at the Ni/TiO_2 interface.

The Cu/Ni surface composition ratio was calculated for bimetallic catalysts after reduction and calcination by summing all contributions to the Cu and Ni 2p3/2 spectra and correction for XPS sensitivity factors. For the Al_2O_3 supported bimetallic catalyst, an almost equal Cu/Ni surface composition ratio of 48.7/51.3 (Table 1) was observed for the reduced catalyst, consistent with the equal weight loadings of Cu and Ni, the miscibility of Cu and Ni, and their expected nonspecific interactions with Al_2O_3.[47,54] Interestingly, the surface composition for the TiO_2 supported bimetallic catalyst was significantly enriched in Cu, with a Cu/Ni ratio of 82.4/17.6. As shown in Table 1 and Figures S4 and S5, the bimetallic catalyst surface compositions were almost identical after reduction and calcination. The surface enrichment of Cu and weaker $Cu–TiO_2$ interactions observed by XPS in the $Cu–Ni/TiO_2$ catalyst compared to monometallic Cu/TiO_2, combined with the observed and well-known stronger interactions between Ni and TiO_2 compared to Cu and TiO_2, suggest that preferential interactions between Ni and TiO_2 drive the formation of core–shell type structures on $Cu–Ni/TiO_2$ catalysts where Cu is preferentially exposed at the surface.

To further substantiate the conclusion that TiO_2 induced the formation of core–shell type structures for the bimetallic catalysts, depth profiling XPS experiments were conducted for reduced $Cu–Ni/TiO_2$ and $Cu–Ni/Al_2O_3$ catalysts by using Ar ion bombardment, Figures 3 and S6 and S7. For the $Cu–Ni/Al_2O_3$ catalyst, an almost constant 50%:50% composition ratio was observed at all Ar sputtering times, which suggests an even distribution of Cu and Ni throughout the bimetallic particles.

DOI: 10.1021/acscatal.7b01095
ACS Catal. 2017, 7, 4070–4082

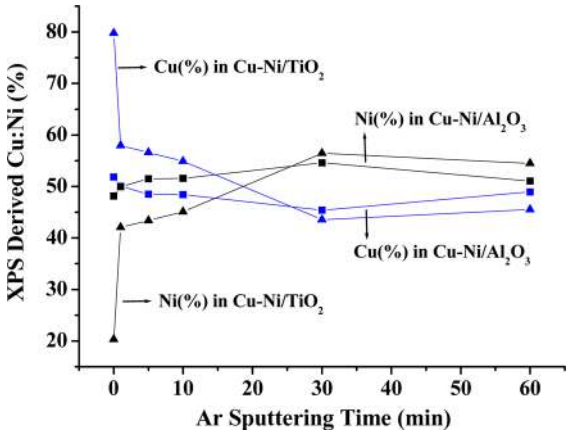

Figure 3. Relative Cu/Ni surface concentration (%) for prereduced Cu−Ni/TiO_2 and Cu−Ni/Al_2O_3 catalysts measured by XPS during depth profiling experiments as a function or Ar sputtering time.

For the Cu−Ni/TiO_2 catalyst, the relative Cu composition decreased from 79.1% to 45.5% as the Ar sputtering time was increased from 0 to 60 min. The switch in composition from predominantly Cu to slightly Ni enriched with increasing Ar sputtering time (and thus depth into the particle) is direct evidence of a core−shell like structure for the TiO_2 supported bimetallic catalysts. Because these catalysts are high surface area materials, a precise relationship between Ar sputtering time and sputtering depth to provide quantitative compositional structure of the particles would be difficult. Regardless of this limitation, contrast between the relative Cu and Ni compositions as a function of Ar sputtering time for the Al_2O_3 and TiO_2 catalysts is strong evidence that TiO_2 induced the formation of core−shell structures where the catalytic surface is Cu enriched and the TiO_2 interface is Ni enriched.

To corroborate inferences regarding metal−support interactions and Cu surface enrichment in Cu−Ni/TiO_2, temperature-programmed reduction (TPR) spectra were measured as shown in Figure 4. The amount of H_2 consumption in the TPR experiments was calculated for all samples, showing relatively consistent values between 1.3 and 1.7 mmol/g catalyst, Table 1, which corresponds to ∼8−10% of the catalyst mass. This is in agreement with the nominal ∼10% metal weight loading in all samples, suggesting that nominal weight loadings well represent the actual weight loadings and that most Cu and Ni species were reduced in the TPR experiments.

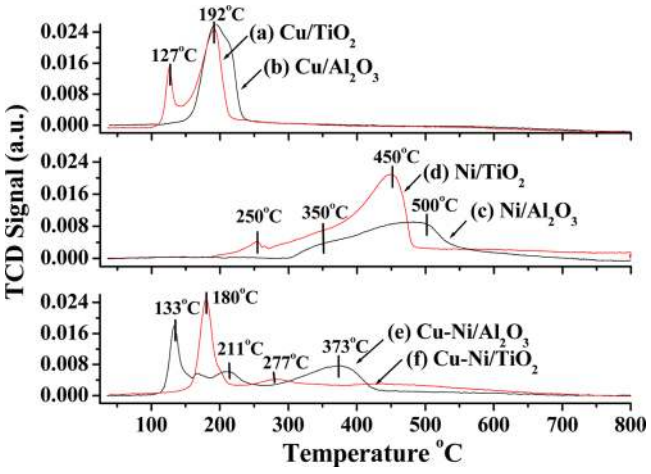

Figure 4. H_2-TPR spectra for (a) Cu/TiO_2, (b) Cu/Al_2O_3, (c) Ni/TiO_2, (d) Ni/Al_2O_3, (e) Cu−Ni/Al_2O_3, and (f) Cu−Ni/TiO_2.

Figure 4a,b show that the TPR spectra of Cu/Al_2O_3 exhibited a single reduction peak at 191 °C, whereas two peaks were observed for Cu/TiO_2 at 127 and 192 °C. The low temperature reduction peak for Cu/TiO_2 is attributed to CuO_x species directly interacting with the TiO_2 support, whereas the ∼190 °C reduction peak is assigned to bulk-like CuO_X.[48] In the case of Ni/Al_2O_3, Figure 4c shows that two reduction peaks were observed at 350 and 500 °C. The former is assigned to the reduction of amorphous NiO species, while the latter is assigned to the reduction of crystalline NiO.[52] Depending on the synthesis procedure and calcination temperature, non-stoichiometric and stoichiometric Ni-aluminates may also form, although these species (TPR peaks >500 °C) were not observed here.[55] The TPR spectra of Ni/TiO_2 in Figure 4d showed three peaks at 250 °C, 350 °C, and 450 °C. The peaks at 250 and 350 °C are assigned to strongly interacting amorphous and crystalline NiO on TiO_2, due to their significant shift down in temperature compared to Ni/Al_2O_3, and the peak at 450 °C is assigned to the onset of TiO_2 reduction.[56] TPR results from the monometallic catalysts are in agreement with XPS results, providing evidence for significant TiO_2 interactions with Cu and Ni and for this interaction being stronger for Ni-TiO_2.

For Cu−Ni/Al_2O_3, the reduction peaks associated with Cu and Ni in Figure 4e both shifted to lower temperatures, as compared to the monometallic catalysts supported on Al_2O_3. This result suggests an intimate interaction between Ni and Cu species, consistent with the TEM and the XPS analyses that showed similar surface concentrations of Cu and Ni.[57,58] For Cu−Ni/TiO_2, the sharp reduction peak observed at 180 °C in Figure 4f was assigned to CuO_x reduction, and the very weak reduction peak at 277 °C was assigned to amorphous NiO reduction. The dominant signature of CuO_x reduction coupled with the lack of peak associated with reduction of CuO_x species that are directly interacting with TiO_2 (seen previously at 127 °C for Cu/TiO_2) are strong evidence of the core−shell structure for Cu−Ni/TiO_2, where Cu is exposed at the surface due to strong Ni−TiO_2 interactions.

To summarize catalyst characterization, monometallic Cu and Ni catalysts on Al_2O_3 and TiO_2 exhibited clear signatures of metal−support charge transfer on TiO_2, and the strength of this interaction was greater for Ni compared to Cu. For the bimetallic catalysts, STEM imaging and elemental mapping showed that all metal particles observed on TiO_2 and Al_2O_3 contained Cu and Ni, demonstrating the formation of bimetallic particles. For Cu−Ni/Al_2O_3, it was observed that the bimetallic particles contained a homogeneous mixture of Cu and Ni throughout the particles. However, for Cu−Ni/TiO_2, strong Ni−TiO_2 interactions induced the formation of core−shell like structures enriched in Cu at the catalytic surface. While it is well documented that surface segregation in bimetallic catalysts can be driven by reactant adsorption, the use of preferential metal−support interactions to control surface compositions in bimetallic catalysts is much less common.[59−61]

3.2. Catalytic Activity. *3.2.1. Hydrogenation of Furfural.* The conversion of FF to MF follows a consecutive reaction pathway with many parallel reactions that can drive formation of undesired products. In addition to catalyst composition, it has been observed that reaction selectivity (and ultimately

DOI: 10.1021/acscatal.7b01095
ACS Catal. 2017, 7, 4070−4082

yields) is sensitive to reaction temperature, time, H_2 pressure, and catalyst/reactant loading. We screened reaction conditions of 180 to 240 °C, 15 to 55 bar H_2, and 5 to 30% catalyst/reactant mass loading ratios to identify the conditions at which both Ni and Cu metals produced the highest MF yields, shown in Figure 5 and Tables S1−S3. It was identified that at a

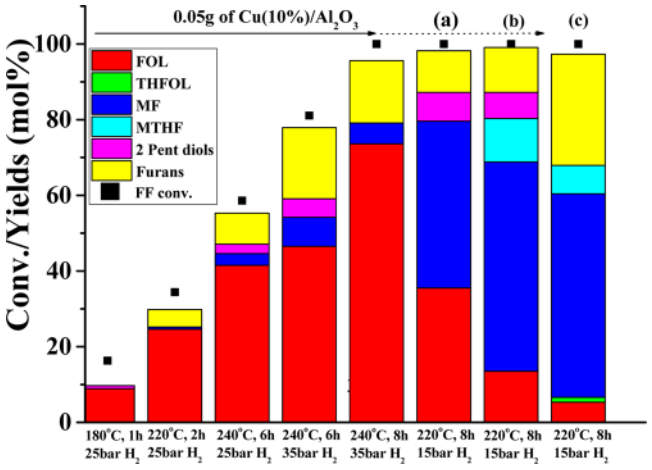

Figure 5. FF conversion and product yields for Cu/Al_2O_3 catalysts for the reaction conditions shown along the *x*-axis at four catalyst loadings. All reactions except those noted by a, b, and c were executed at a FF loading of 1 g, 25 mL of IPA solvent, and a Cu(10 wt %)/Al_2O_3 catalyst loading of 0.05 g. The catalyst loadings for the other three were (a) 0.15 g for Cu (10 wt %)/Al_2O_3], (b) 0.3 g for Cu (10 wt %)/Al_2O_3, and (c) 0.3 g for Cu (25 wt %)/Al_2O_3.

temperature of 200 °C, 25 bar of H_2 pressure, and a catalyst/reactant loading of 30%, decarbonylation and ring opening reactions were significantly suppressed, and the reactions on all catalysts were mostly by hydrogenation and hydrogenolysis of FF. All subsequent reactions were performed under these conditions. It is also worth noting that for initial catalyst screening, isopropyl alcohol was used as a solvent. However, because of significant solvent conversion, all subsequent reactivity comparisons used 1,4-dioxane as the solvent due to its stability under optimized reaction conditions.

The conversion of FF and yield of various products over monometallic Ni and Cu on Al_2O_3 and TiO_2 catalysts at 1 and 8 (4 for Ni) hour reaction times is shown in Figure 6. Generally, monometallic Cu catalysts were selective for MF production, while Ni catalysts were selective for production of THFOL.[62] The Ni catalysts were significantly more reactive than Cu catalysts, as evidenced by the ∼1 order of magnitude longer reaction time required for full FF conversion on Cu. On the Ni/Al_2O_3 catalyst, FF was completely converted with a 54.5% yield of THFOL and 30.5% yield of MF after 1 h, and the product selectivity did not change after 4 h. The Ni/TiO_2 catalyst was less active than Ni/Al_2O_3, with some FOL remaining after 1 h and the product selectivity stabilizing after ∼4 h with 70% yield of THFOL and ∼15% yield of MF. THFOL as the primary product over the Ni catalyst is consistent with the known strong interactions between the furan ring in FF and Ni surfaces, which drives ring hydrogenation.[62,63] The strong interactions between Ni and TiO_2 observed by XPS and TPR and the enhanced THFOL yields on Ni/TiO_2 compared to Ni/Al_2O_3 indicate that Ni sites near the TiO_2 interface coordinate more selectively with the furan ring in FF rather than the carbonyl (or subsequently

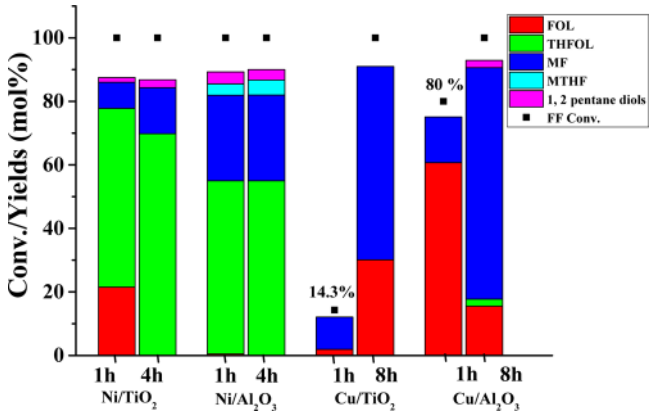

Figure 6. FF conversion and product yields over monometallic Ni and Cu supported on Al_2O_3 and TiO_2 catalysts at different reaction times. All reactions were run with an FF loading of 1 g, a catalyst loading of 0.3 g, 25 mL of 1,4-dioxane as a solvent, a temperature of 200 °C, and an H_2 pressure of 25 bar.

produced alcohol) group, thus promoting ring hydrogenation rather than carbonyl hydrogenolysis.

Cu catalysts were much less active than Ni catalysts and required ∼8 h to achieve complete FF conversion, likely due to their weak ability to activate H_2.[64] Similar to the Ni catalysts, Cu/Al_2O_3 was more active than Cu/TiO_2. Figure 6 shows that for Cu/Al_2O_3 41% of FF was converted to yield 21.5% FOL and 17.2% MF at 1 h, while for Cu/TiO_2, 25.7% of FF was converted to yield 12.1% FOL and 12.7% MF at 1 h. Further extending reaction times to 8 h resulted in complete FF conversion for both catalysts with similar final MF yields of 74.9% for Cu/Al_2O_3 and 75.9% for Cu/TiO_2. THFOL yields were suppressed on Cu catalysts compared to Ni, due to repulsive interactions between the Cu 3d band and the aromatic furan ring.[25] To more effectively compare FF conversion on the monometallic Cu catalysts, Figure S8 shows FF conversion and product yields over time on both the Cu/Al_2O_3 and Cu/TiO_2 catalysts. In both cases, the time dependent yield profile of FOL strongly suggests that this species is an intermediate in the production of MF, as previously reported.[32,65] There were slight differences in the time dependent yields of FOL and MF for the Cu/TiO_2 and Cu/Al_2O_3 catalysts, particularly at all times <6 h for which higher yields of FOL are realized on Cu/Al_2O_3 than on Cu/TiO_2. These results suggest that the initial hydrogenation of FF to FOL occurs more effectively on Cu/Al_2O_3, whereas the hydrogenolysis of FOL to form MF occurs more readily on Cu/TiO_2. Although Cu/Al_2O_3 is more active than Cu/TiO_2, small amounts of undesired products such as diols and pentanols were obtained at an 8 h reaction time on Cu/Al_2O_3. Differences in reactivity of the monometallic Cu catalysts were likely caused by interactions between Cu and the support, which can change the charge state of the active metal or introduce interfacial reaction pathways and the inherent acidity of the support.[44,45] Comparing Ni and Cu catalysts, it is clear that Ni promotes ring hydrogenation to form THFOL, while Cu is selective for hydrogenolysis to form the desired product MF and that the support composition only mildly influenced catalyst performance.

While the nature of the support induced relatively small changes in the reactivity of monometallic Cu and Ni catalysts, the support significantly influenced the selectivity and reactivity of FF conversion for the Cu−Ni bimetallic catalysts, as shown

DOI: 10.1021/acscatal.7b01095
ACS Catal. 2017, 7, 4070−4082

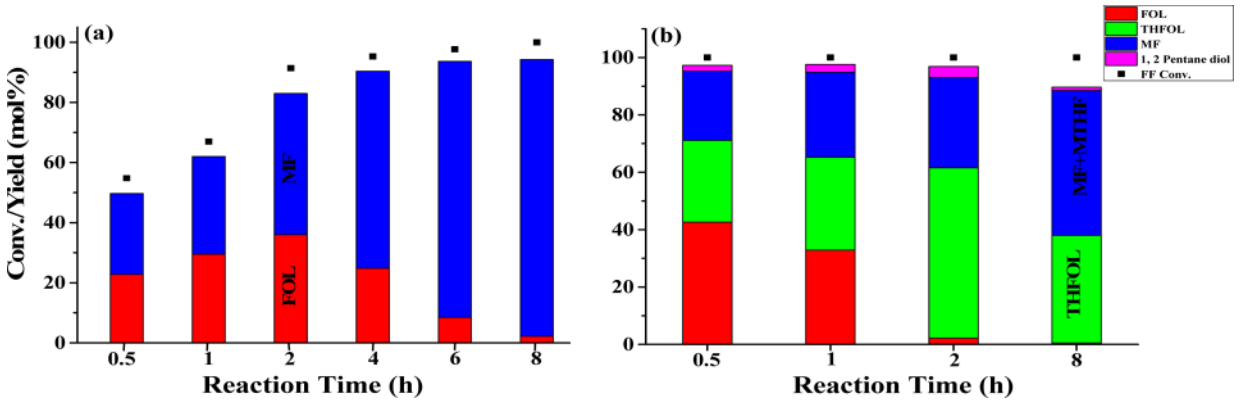

Figure 7. FF conversion and product yields as a function of reaction time over (a) Cu−Ni/TiO_2 and (b) Cu−Ni/Al_2O_3 catalysts. All reactions were run at a FF loading of 1 g, a catalyst loading of 0.3 g, and 25 mL of 1,4-dioxane as a solvent at a temperature of 200 °C and H_2 pressure of 25 bar.

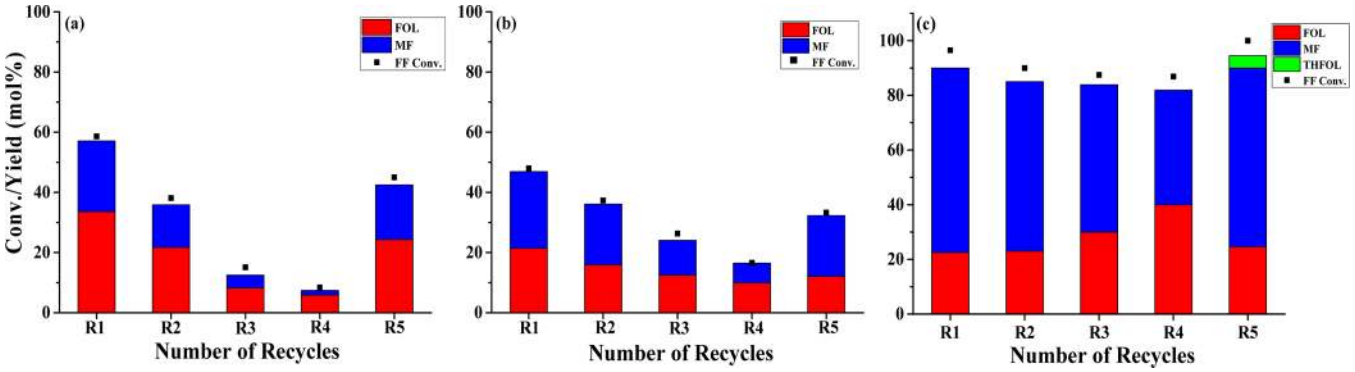

Figure 8. FF conversion and product yields as a function of number of catalyst recycles, R, for (a) Cu/Al_2O_3, (b) Cu/TiO_2, and (c) Cu−Ni/TiO_2 catalysts. After R4, catalysts were calcined at 450 °C for 5 h and reduced at 450 °C for 3 h prior to R5. Reaction conditions were a FF loading of 1 g, catalyst loading of 0.3 g, 25 mL of 1,4-dioxane as a solvent, a temperature of 200 °C, H_2 pressure of 25 bar, and 2 h run time.

in Figure 7. Cu−Ni/Al_2O_3 was more active than Cu−Ni/TiO_2 with 100% FF conversion achieved in 0.5 h reaction time for Cu−Ni/Al_2O_3, whereas 8 h was required for complete FF conversion on Cu−Ni/TiO_2. On Cu−Ni/TiO_2, MF and FOL were the primary products, with MF selectivity increasing with reaction time to ultimately achieve a 92.1% yield of MF at 8 h. Conversely, the Cu−Ni/Al_2O_3 catalysts favored furan ring hydrogenation, which resulted in increasing THFOL yields with a subsequent loss of FOL, as reaction time was extended. When comparing results with Cu−Ni/Al_2O_3 to those with monometallic Ni and Cu catalysts, both the reactivity (time for complete FF conversion) and product distribution (primarily THFOL, MF, and at short times FOL) strongly resembled the behavior of the monometallic Ni catalysts. Cu−Ni/TiO_2 showed reactivity behavior that was more similar to that of Cu, with only MF and FOL as significant products. However, Cu−Ni/TiO_2 exhibited about 2-fold higher conversion at the same reaction time compared to monometallic Cu/TiO_2 and significantly enhanced MF yields at longer reaction times (92% vs 75.9%).

Issues previously identified for the application of Cu-based catalysts to FF HDO are the potential for Cu sintering or carbon deposition affecting stability at reaction conditions. To examine these effects, recycle and regeneration experiments were performed where four sequential reactivity experiments were executed without treating the catalyst between experiments, followed by calcination and reduction of the catalysts prior to a final reactivity experiment. It is expected that a loss in reactivity during the four sequential experiments could be due to carbon deposits and Cu sintering, while regeneration should predominantly remove carbonaceous deposits, allowing differentiation of the catalyst degradation mechanisms. As shown in Figure 8a, using the Cu/Al_2O_3 catalyst, FF conversion dropped from 56% to 10% by the fourth reactivity experiment (R4) and then increased to ∼47% after a regeneration step (R5), whereas MF selectivity was relatively similar in the first (R1) and fifth (R5) experiments, Figure 8a. The results are consistent with previous studies of Cu/Al_2O_3 catalysts showing low stability under FF HDO conditions.[66−68] For Cu/TiO_2, the FF conversion decreased from 47% to 18% by R4 but increased to 37% following regeneration (R5), with a similar selectivity to R1, Figure 8b. The lower loss of reactivity during the four sequential experiments (R1−R4) for Cu/TiO_2 compared to Cu/Al_2O_3 suggests that the amount of carbonaceous deposits is reduced by the use of TiO_2 as a support. However, the similar change in reactivity comparison of R1 and R5 for Cu/TiO_2 and Cu/Al_2O_3 suggests that Cu sintering similarly occurs for both catalysts.

For the Cu−Ni/TiO_2 catalyst, FF conversion decreased from 93.5 to 85.1% from R1 to R4, demonstrating enhanced stability compared to the monometallic Cu catalysts, Figure 8c. Regeneration of Cu−Ni/TiO_2 restored the MF and FOL yields seen in the initial experiment, although a small amount of THFOL formation was also observed. The results demonstrate that Cu−Ni/TiO_2 catalysts exhibit significantly increased resistance to reactivity degradation caused by carbon deposition and sintering compared to Cu/TiO_2 and Cu/Al_2O_3. However, it was also observed that a combination of exposure to reaction

DOI: 10.1021/acscatal.7b01095
ACS Catal. 2017, 7, 4070−4082

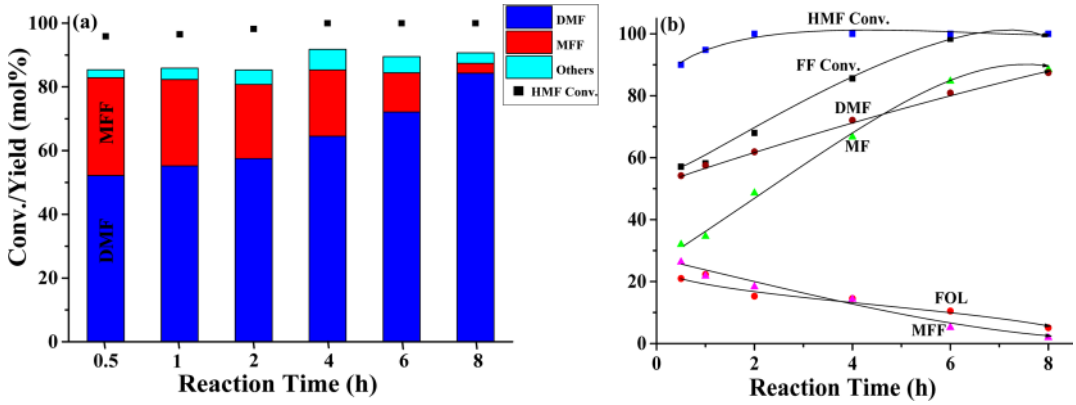

Figure 9. (a) HMF and (b) HMF + FF conversion and product yields as a function of reaction time over the Cu−Ni/TiO_2 catalyst. For a, reactions were run at an HMF loading of 0.5 g, a catalyst loading of 0.3 g, 25 mL of 1,4-dioxane as the solvent, a temperature of 200 °C, and a H_2 pressure of 25 bar. For b, reactions were run at an FF loading of 0.5 g, HMF loading of 0.25 g, catalyst loading of 0.3 g, 25 mL of 1,4-dioxane as the solvent, a temperature of 200 °C, and an H_2 pressure of 25 bar.

conditions and regeneration of the Cu−Ni/TiO_2 catalyst resulted in the exposure of small amounts of surface Ni domains that drive ring hydrogenation.

3.2.2. HDO of HMF and Coprocessing of FF and HMF. Because Cu−Ni/TiO_2 showed excellent reactivity, MF selectivity, and stability for FF conversion, this catalyst was further tested for reactivity in HMF conversion to DMF and simultaneous coprocessing of HMF and FF to DMF and MF, respectively. The measured time dependent conversion of HMF and HMF with FF (coprocessing) and product yields on Cu−Ni/TiO_2 are shown in Figure 9a and b, respectively. HMF conversion to DMF is known to occur through two reaction pathways.[43] In the first pathway, hydrogenolysis of HMF yields methyl furfural (MFF) and then hydrogenation followed by hydrogenolysis of MFF to DMF, as shown in Scheme 2. In a second pathway, 2,5-bis(hydroxymethyl) furan (BHMF) is the intermediate product, and further hydrogenation of both C−O groups in BHMF results in DMF formation. The conversion of either BHMF or MFF to DMF typically occurs through methylfurfuryl alcohol (MFOL), per Scheme 2. However, MFOL is highly reactive and immediately converts into DMF by hydrogenolysis.[45]

For HMF conversion over Cu−Ni/TiO_2, 95.9% conversion of HMF was observed within 0.5 h of reaction, with the primary products being DMF (52.2% yield) and MFF (30.7% yield). With increasing reaction times, MFF was converted selectively to DMF to ultimately result in 84.3% yield of DMF at 8 h of reaction time. Small amounts of MFOL were also observed as a rapidly converted intermediate in the production of DMF from MFF.

In the coprocessing of HMF and FF over Cu−Ni/TiO_2, 0.5 g of FF and 0.250 g of HMF were used as reactants with 0.3 g of the catalyst under the same reaction conditions as the HMF and FF cases. Cu−Ni/TiO_2 showed similar activity and methylated furan (MF + DMF) yields as in individual processing of HMF and FF. Moreover, based on the time dependent yields of intermediate products (FOL and MFF, for example), the mechanism of methylated furan production did not change for coprocessing of FF and HMF. The maximum yields of MF (88.5%) and DMF (87.5%) were realized after 8 h of reaction at very similar yields to those for the individual processing cases.

Summarizing the reactivity results, the monometallic Cu and Ni catalysts showed FF hydrogenation and HDO reactivity consistent with previous reports, and their reactivity exhibited minimal sensitivity to support composition.[23,65,69] However, the bimetallic Cu−Ni catalysts showed significant support effects for FF HDO. On Al_2O_3, the bimetallic catalyst acted similarly to Ni alone, while on TiO_2, the Cu−Ni bimetallic catalyst enhanced rates and MF selectivity compared to Cu alone. The Cu−Ni/TiO_2 catalyst showed good stability, regenerability, reactivity, and MF selectivity and outperformed monometallic Cu catalysts in all performance metrics under similar conditions.[41,43] Finally, Cu−Ni/TiO_2 showed excellent selectivity toward methylated furans in HMF and FF/HMF coprocessing reactions.

4. DISCUSSION

The significant support effect observed for bimetallic Cu−Ni catalysts can be explained and rationalized through the catalyst characterization studies. Cu−Ni/Al_2O_3 reactivity studies suggested that the behavior of the catalyst significantly resembled pure Ni catalysts, where ring hydrogenation was prevalent. Both TPR and XPS showed evidence of equal amounts of Cu and Ni exposed at the catalyst surfaces, while the TEM images suggested that all catalytic particles contained Ni and Cu. On Ni, the primary η^2(C═O) FF adsorption geometry brings the aromatic ring close to the surface, enabling ring hydrogenation (Figure 10).[44,70,71] Because the ring-surface interaction is only expected at Ni surface domains that have Ni ensemble sizes large enough to coordinate to the furan ring, or at Cu−Ni alloy surface structures with electronic structures significantly resembling monometallic Ni, it can be concluded that Ni-rich domains at the surface of bimetallic Cu−Ni particles were responsible for a majority of the reactivity of the Cu−Ni/Al_2O_3 catalyst. The proposed Cu−Ni bimetallic particle structure on Al_2O_3 based on the XPS measurements and reactivity results is shown schematically in Figure 10.

The Cu−Ni/TiO_2 catalyst reactivity significantly resembled that of Cu alone, albeit with enhanced reaction rates and MF selectivity. This result can be explained based on the depth profiling XPS, TPR, and TEM results, which together suggest that TiO_2 supported bimetallic Cu−Ni particles segregate into core−shell geometries that preferentially expose Cu at their surface, as shown schematically in Figure 10. On Cu surfaces, the FF ring is repelled from the surface due to the full valence d-band, forming the η^1(O) FF adsorption geometry, and thus, as opposed to Ni surfaces, carbonyl hydrogenation is favored

DOI: 10.1021/acscatal.7b01095
ACS Catal. 2017, 7, 4070−4082

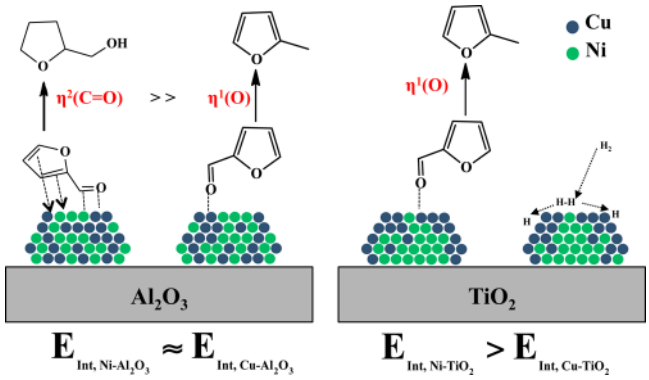

Figure 10. Schematic diagram of the proposed operating states of Cu−Ni bimetallic catalysts on Al_2O_3 and TiO_2. For Cu−Ni/Al_2O_3, significant exposure of extended Ni domains drives efficient ring hydrogenation to form THFOL, whereas the segregated structure of Cu−Ni on TiO_2 facilitates MF formation. E_{INT}: Energy of interaction between metal (either Ni or Cu) and support (Al_2O_3 and TiO_2).

on Cu over ring hydrogenation. The enhanced reactivity and MF selectivity on Cu−Ni/TiO_2 compared to monometallic Cu catalysts, with no additional ring hydrogenation or decarbonylation, is primarily attributed to increased rates of H_2 dissociation.[33,64] The enhanced rates of H_2 dissociation but retained Cu selectivity characteristics could occur at so-called single atom surface alloys, where small collections (1−3, essentially small enough so they cannot coordinate to a furan ring) of Ni atoms are exposed at the Cu surface to allow for enhanced H_2 dissociation rates but not the η^2(C═O) FF adsorption geometry.[64,72,73] These reactivity characteristics could also be consistent with a low relative Ni concentration near surface alloy that electronically or sterically modifies the exposed surface Cu atoms and enables enhanced H_2 dissociation rates.[74,75] Although we cannot differentiate these two mechanisms, it is clear that Cu was significantly enriched at the surface in Cu−Ni/TiO_2 catalysts, yet still modified by Ni in a manner that enhanced H_2 dissociation rates without changes in the inherent preference of Cu for carbonyl hydrogenolysis over ring hydrogenation (see Figure 10).

The above discussion, combined with the weak influence of the support composition on the reactivity of the monometallic catalysts, strongly suggests that the primary role of TiO_2 in promoting the catalytic properties of the Cu−Ni catalyst is indirect, with Ni driven to the TiO_2 interface and Cu preferentially exposed at the surface. Thus, TiO_2 controls the bimetallic Cu−Ni catalyst surface composition but does not directly participate in the catalytic process.[76,77] A well-known behavior on TiO_2 supported Pt-group metal catalysts is strong metal support interactions (SMSI), where support reduction (oxygen vacancy formation) drives TiO_2 encapsulation of the active metal particle.[78−80] While a metal selective SMSI encapsulation state that preferentially encapsulates Ni could be imagined, the TPR data oppose this interpretation. SMSI encapsulation states with TiO_2 are typically observed following >500 °C reduction treatment. Because minimal Ni reduction peaks were observed for the Cu−Ni/TiO_2 catalysts despite Ni reduction peaks being clearly observable in the Ni-TiO_2 catalyst, Ni is likely buried subsurface in the bimetallic particles prior to SMSI encapsulation layer formation. This mechanism is further supported by the XPS analysis of surface composition in the prereduced and preoxidized Cu−Ni/TiO_2 catalysts that show identical Cu/Ni surface concentration ratios in Table 1. Thus, preferential interactions between Ni and TiO_2 are believed to drive the formation of core−shell like particles where Cu is primarily exposed at the catalyst surface, see proposed structures in Figure 10. We propose that support induced bimetallic particle segregation may be quite general for reducible oxide supported bimetallic catalysts, given known metal specific interactions with reducible supports.[79]

The structural properties of Cu−Ni alloys have been extensively studied for their potential application to a range of reactions.[81−89] Bulk Cu−Ni alloys are miscible and equilibrated into alloy phases when heated above ∼400 °C.[90] In bulk systems (polycrystalline films, single crystalline films, and other structures), Cu surface segregation has been reported to be due to the lower surface energy of Cu in a vacuum compared to Ni.[84,91−95] It has further been demonstrated that the surface segregation is a facet dependent phenomenon that occurs more predominantly on (100) surface facets compared to (111) surface facets.[92,96] Insights into the structure of bulk Cu−Ni alloys have not translated into a complete understanding of the structure of supported Cu−Ni alloy nanoparticles, where multiple surface facets are simultaneously exposed, and the distribution of Cu and Ni is also influenced by interfacial interactions with the support and environment.

Previous reports of 50%−50% Cu−Ni alloy nanoparticles supported on irreducible supports (SiO_2 and Al_2O_3) have found that as-synthesized particles show no evidence of Cu surface segregation.[47,54,89,97,98] However, reports of Cu−Ni alloy nanoparticles on reducible supports (CeO_2, ZrO_2, MgO), or supports with significant surface defect concentrations (SBA-15), have shown evidence of Cu enriched surfaces, in agreement with our findings.[49,88,99,100] Thus, while bulk Cu−Ni alloys exhibit Cu surface segregation due to the decreased surface energy of Cu in a vacuum, it seems that for supported Cu−Ni alloy nanoparticles, preferential Ni-support interactions on reducible or defective supports is the primary driving force for Cu surface segregation. Also, reconstruction of the as-synthesized catalytic structure under reaction conditions may be expected when significant adsorbate−metal specific interactions exist, for example in a CO atmosphere.[89] However, based on the lack of ring hydrogenation observed in our studies for the Cu−Ni/TiO_2 catalyst, it can be concluded that migration of Ni to the catalyst surface is minimal under reaction conditions.

It is worth comparing our results to recent reports that examined the influence of modification of Cu catalysts with Ni on reactivity in FF HDO. A surface science approach was used to compare pure Cu (111) and Ni (111) surfaces with a Ni surface layer on Cu (111) and a Cu surface layer on Ni (111) for FF hydrogenation.[101] It was clearly seen that in both surface layer configurations, bimetallics enhanced selectivity toward MF formation compared to monometallics. However, even in the case of Cu monolayers on Ni (111), significant nonselective decomposition of FF was observed. This result suggests that for the Cu−Ni/TiO_2 catalysts examined here, the Ni concentration in the near surface region is much lower than for the prior surface science study. A separate study of the influence of Ni addition at various concentrations to Cu/Al_2O_3 on FF hydrogenation reactivity and selectivity[33] showed that increasing the Ni loading increased the rate of FF conversion but also increased the selectivity toward ring hydrogenation, decarbonylation, and ring opening products. The introduction of self-assembled organic monolayers to the catalyst lowered the Ni surface content in Cu−Ni/Al_2O_3, thereby boosting selectivity

DOI: 10.1021/acscatal.7b01095
ACS Catal. 2017, 7, 4070−4082

and reaction rate for hydrogenation products (we note that FOL was the main product in these studies, which is likely caused by the reactions being performed in the gas phase). In this case, it seems that the use of self-assembled monolayers to control the exposed surface concentration of Ni in bimetallic Cu−Ni catalysts bears some resemblance to our reported use of TiO_2 to control the Ni surface concentration in bimetallic Cu−Ni catalysts. Although, the Cu−Ni/TiO_2 catalysts reported here enable complete conversion and high yields to MF and are expected to have enhanced stability compared to the organic functionalized Cu−Ni catalysts reported previously, thus creating a more scalable approach for controlling Cu surface chemistry for selective hydrogenation reactions. In addition, it was very recently reported that increasing the Ni content in Cu−Ni/MgAlO catalysts enhanced FF conversion (>99%); however, FOL and THFOL were the only selective products observed.[58]

In addition to considering how TiO_2 induced segregation of Cu−Ni catalyst particles influenced reactivity and selectivity, it is also interesting to explore how this factor may have influenced stability and catalyst regeneration. In the recycling-regeneration experiments shown in Figure 8, it was observed that the Cu/TiO_2 and Cu/Al_2O_3 catalysts exhibited similar performance degradation that is ascribed to carbonaceous deposits on the metal and Cu sintering. The improved stability of Cu−Ni/TiO_2 compared to the monometallic catalysts during recycle experiments (R1−R4) is likely due to decreased carbon deposition on the catalysts driven by increased H_2 dissociation rates. Increased stability of the Cu−Ni/TiO_2 catalyst compared to the monometallic Cu catalysts when considering R1 and R5 is likely due to reduced sintering of the active Cu metal. This suggests that Ni serves as an anchoring site for Cu on TiO_2, which enhances catalyst stability and provides a stable platform for regeneration of the core−shell Cu−Ni structure to that for high MF selectivity and reactivity. Further reduction of the Ni loading in Cu−Ni/TiO_2 catalysts may allow for similar enhanced reactivity and stability as observed here while also minimizing the surface exposure of Ni observed with increased time under reaction conditions.

Recently, it has been shown that cosolvent-enhanced lignocellulosic fractionation (CELF) of raw biomass enables the production of HMF and FF with extremely high yields.[11] Separation of HMF and FF in a liquid stream from the remaining lignin can be effectively achieved through various approaches to yield a combined stream of HMF and FF that is typically rich in FF. Our demonstration of high yield, single pot conversion of FF and HMF over stable and regenerable Cu−Ni/TiO_2 catalysts opens new possibilities for an efficient and high yield biomass to the fuel conversion process with only a few required process steps. It is expected that coupling of CELF pretreatment of cellulosic biomass with FF/HMF catalytic coprocessing will enable an effective approach for conversion of raw biomass to high quality fuels.

5. CONCLUSIONS

In conclusion, our study showed that Cu−Ni/TiO_2 enabled high yield (~90%) conversion of FF and HMF to methylated furans in either single or coprocessing schemes, results not possible with monometallic Cu and Ni, or Cu−Ni/Al_2O_3. The reactivity of Cu−Ni/TiO_2 is proposed to result from strong and selective Ni−TiO_2 interactions that favored the formation of the Cu-shell and Ni-core structures, allowing for high selectivity in HDO and enhanced reactivity compared to monometallic Cu catalysts. Furthermore, the strong Ni−TiO_2 interactions effectively anchored the bimetallic particles to the TiO_2 support, thereby reducing catalyst degradation via sintering and enabling effective regeneration. Finally, it is envisioned that a potentially economical biomass to fuel conversion process can be achieved by coupling CELF pretreatment of raw biomass to produce high yield liquid streams of HMF and FF with catalytic coprocessing using Cu−Ni/TiO_2 to high yields of methylated furans.

■ ASSOCIATED CONTENT

Supporting Information

The Supporting Information is available free of charge on the ACS Publications website at DOI: 10.1021/acscatal.7b01095.

Additional catalyst characterization (XRD, TEM, XPS) and reactivity data provided in Figures S1−S8 and Tables S1−S3 (PDF)

■ AUTHOR INFORMATION

Corresponding Author

*E-mail: christopher@engr.ucr.edu.

ORCID

Phillip Christopher: 0000-0002-4898-5510

Notes

The authors declare no competing financial interest.

■ ACKNOWLEDGMENTS

The authors acknowledge funding support from DOE-EERE BETO Office through Award DE-EE0007006. The authors acknowledge Dr. Krassimir N. Bozhilov for assistance with the electron microscopy performed at the CFAMM at UC Riverside. Dr. Ilkeun Lee is acknowledged for assistance with the XPS analysis made possible by NSF grant DMR-0958796.

■ REFERENCES

(1) Lynd, L. R.; Laser, M. S.; Bransby, D.; Dale, B. E.; Davison, B.; Hamilton, R.; Himmel, M.; Keller, M.; McMillan, J. D.; Sheehan, J.; Wyman, C. E. *Nat. Biotechnol.* **2008**, *26*, 169−172.

(2) Huber, G. W. *Science* **2005**, *308*, 1446−1450.

(3) Perlack, R. D.; Stokes, B. J.; Eaton, L. M.; Turnhollow, A. F. *U.S. Billion-Ton Update, Biomass Supply for a Bioenergy and Bioproducts Industry*; U.S. Department of Energy, Oak Ridge National Laboratory: Oak Ridge, TN, 2011; pp 1−229.

(4) Kunkes, E. L.; Simonetti, D. A.; West, R. M.; Serrano-ruiz, J. C.; Gärtner, C. A.; Dumesic, J. A. *Science* **2008**, *322*, 417−421.

(5) Gürbüz, E. I.; Alonso, D. M.; Bond, J. Q.; Dumesic, J. A. *ChemSusChem* **2011**, *4*, 357−361.

(6) Nakagawa, Y.; Tamura, M.; Tomishige, K. *ACS Catal.* **2013**, *3*, 2655−2668.

(7) Huber, G. W.; Iborra, S.; Corma, A. *Chem. Rev.* **2006**, *106*, 4044−4098.

(8) Seemala, B.; Haritos, V.; Tanksale, A. *ChemCatChem* **2016**, *8*, 640−647.

(9) Zhang, T.; Kumar, R.; Wyman, C. E. *Carbohydr. Polym.* **2013**, *92*, 334−344.

(10) Cai, C. M.; Zhang, T.; Kumar, R.; Wyman, C. E. *Green Chem.* **2013**, *15*, 3140−3145.

(11) Cai, C. M.; Nagane, N.; Kumar, R.; Wyman, C. E. *Green Chem.* **2014**, *16*, 3819−3829.

(12) Schmidt, L. D.; Dauenhauer, P. J. *Nature* **2007**, *447*, 914−915.

(13) Bond, J. Q.; Upadhye, A. a.; Olcay, H.; Tompsett, G. A.; Jae, J.; Xing, R.; Alonso, D. M.; Wang, D.; Zhang, T.; Kumar, R.; Foster, A.; Sen, S. M.; Maravelias, C. T.; Malina, R.; Barrett, S. R. H.; Lobo, R.;

DOI: 10.1021/acscatal.7b01095
ACS Catal. 2017, 7, 4070−4082

Wyman, C. E.; Dumesic, J. A.; Huber, G. W. *Energy Environ. Sci.* **2014**, *7*, 1500−1523.
(14) Matson, T. D.; Barta, K.; Iretskii, A. V.; Ford, P. C. *J. Am. Chem. Soc.* **2011**, *133*, 14090−14097.
(15) De, S.; Zhang, J.; Luque, R.; Yan, N. *Energy Environ. Sci.* **2016**, *9*, 3314−3347.
(16) Gawande, M. B.; Goswami, A.; Felpin, F. X.; Asefa, T.; Huang, X.; Silva, R.; Zou, X.; Zboril, R.; Varma, R. S. *Chem. Rev.* **2016**, *116*, 3722−3811.
(17) Li, D.; Atake, I.; Shishido, T.; Oumi, Y.; Sano, T.; Takehira, K. *J. Catal.* **2007**, *250*, 299−312.
(18) Climent, M. J.; Corma, A.; Iborra, S. *Green Chem.* **2011**, *13*, 520−540.
(19) Lin, Y.-C.; Huber, G. W. *Energy Environ. Sci.* **2009**, *2*, 68−80.
(20) Srivastava, R. D.; Guha, A. K. *J. Catal.* **1985**, *91*, 254−262.
(21) Li, X.; Jia, P.; Wang, T. *ACS Catal.* **2016**, *6*, 7621−7640.
(22) Mariscal, R.; Maireles-Torres, P.; Ojeda, M.; Sádaba, I.; López Granados, M. *Energy Environ. Sci.* **2016**, *9*, 1144−1189.
(23) Nagaraja, B. M.; Padmasri, A. H.; David Raju, B.; Rama Rao, K. S. *J. Mol. Catal. A: Chem.* **2007**, *265*, 90−97.
(24) Rao, R. S.; Baker, T. K.; Vannice, M. A. *Catal. Lett.* **1999**, *60*, 51−57.
(25) Sitthisa, S.; Sooknoi, T.; Ma, Y.; Balbuena, P. B.; Resasco, D. E. *J. Catal.* **2011**, *277*, 1−13.
(26) Vargas-Hernández, D.; Rubio-Caballero, J. M.; Santamaría-González, J.; Moreno-Tost, R.; Mérida-Robles, J. M.; Pérez-Cruz, M. A.; Jiménez-López, A.; Hernández-Huesca, R.; Maireles-Torres, P. *J. Mol. Catal. A: Chem.* **2014**, *383*−*384*, 106−113.
(27) Rao, R.; Dandekar, A.; Baker, R. T. K.; Vannice, M. A. *J. Catal.* **1997**, *171*, 406−419.
(28) Yan, K.; Chen, A. *Fuel* **2014**, *115*, 101−108.
(29) Zheng, H. Y.; Zhu, Y. L.; Teng, B. T.; Bai, Z. Q.; Zhang, C. H.; Xiang, H. W.; Li, Y. W. *J. Mol. Catal. A: Chem.* **2006**, *246*, 18−23.
(30) Dong, F.; Zhu, Y.; Ding, G.; Cui, J.; Li, X.; Li, Y. *ChemSusChem* **2015**, *8*, 1534−1537.
(31) Stevens, J. G.; Bourne, R. A.; Twigg, M. V.; Poliakoff, M. *Angew. Chem., Int. Ed.* **2010**, *49*, 8856−8859.
(32) Sheng, H.; Lobo, R. F. *ChemCatChem* **2016**, *8*, 3402−3408.
(33) Pang, S. H.; Love, N. E.; Medlin, J. W. *J. Phys. Chem. Lett.* **2014**, *5*, 4110−4114.
(34) Wu, J.; Gao, G.; Li, J.; Sun, P.; Long, X.; Li, F. *Appl. Catal., B* **2017**, *203*, 227−236.
(35) Lange, J. P.; Van Der Heide, E.; Van Buijtenen, J.; Price, R. *ChemSusChem* **2012**, *5*, 150−166.
(36) Hu, L.; Tang, X.; Xu, J.; Wu, Z.; Lin, L.; Liu, S. *Ind. Eng. Chem. Res.* **2014**, *53*, 3056−3064.
(37) Luo, J.; Arroyo-Ramírez, L.; Wei, J.; Yun, H.; Murray, C. B.; Gorte, R. J. *Appl. Catal., A* **2015**, *508*, 86−93.
(38) Luo, J.; Yun, H.; Mironenko, A. V.; Goulas, K.; Lee, J. D.; Monai, M.; Wang, C.; Vorotnikov, V.; Murray, C. B.; Vlachos, D. G.; Fornasiero, P.; Gorte, R. J. *ACS Catal.* **2016**, *6*, 4095−4104.
(39) Nagpure, A. S.; Lucas, N.; Chilukuri, S. V. *ACS Sustainable Chem. Eng.* **2015**, *3*, 2909−2916.
(40) Román-Leshkov, Y.; Barrett, C. J.; Liu, Z. Y.; Dumesic, J. A. *Nature* **2007**, *447*, 982−985.
(41) Thananatthanachon, T.; Rauchfuss, T. B. *Angew. Chem., Int. Ed.* **2010**, *49*, 6616−6618.
(42) Zhu, Y.; Kong, X.; Zheng, H.; Ding, G.; Zhu, Y.; Li, Y.-W. *Catal. Sci. Technol.* **2015**, *5*, 4208−4217.
(43) Guo, W.; Liu, H.; Zhang, S.; Han, H.; Liu, H.; Jiang, T.; Han, B.; Wu, T. *Green Chem.* **2016**, *18*, 6222−6228.
(44) Kong, X.; Zheng, R.; Zhu, Y.; Ding, G.; Zhu, Y.; Li, Y. *Green Chem.* **2015**, *17*, 2504−2514.
(45) Huang, Y. B.; Chen, M. Y.; Yan, L.; Guo, Q. X.; Fu, Y. *ChemSusChem* **2014**, *7*, 1068−1072.
(46) Wu, Q.; Duchstein, L. D. L.; Chiarello, L.; Christensen, J. M.; Damsgaard, C. D.; Elkjær, C. F.; Wagner, J. B.; Temel, B.; Grunwaldt, J.-D.; Jensen, A. D. *ChemCatChem* **2014**, *6*, 301−310.
(47) Naghash, A. R.; Etsell, T. H.; Xu, S. *Chem. Mater.* **2006**, *18*, 2480−2488.
(48) Larsson, P. O.; Andersson, A. *J. Catal.* **1998**, *179*, 72−89.
(49) Wolfbeisser, A.; Kovács, G.; Kozlov, S. M.; Föttinger, K.; Bernardi, J.; Klötzer, B.; Neyman, K. M.; Rupprechter, G. *Catal. Today* **2017**, *283*, 134−143.
(50) Park, J.; Jung, Y.; Cho, J.; Choi, W. *Appl. Surf. Sci.* **2006**, *252*, 5877−5891.
(51) Larsson, P.-O.; Andersson, A.; Wallenberg, L. R.; Svensson, B. *J. Catal.* **1996**, *163*, 279−293.
(52) Biesinger, M. C.; Payne, B. P.; Lau, L. W. M.; Gerson, A.; Smart, R. S. C. *Surf. Interface Anal.* **2009**, *41*, 324−332.
(53) Pan, J. S.; Tao, J. G.; Huan, C. H. A.; Chiam, S. Y.; Zhang, Z.; Li, D. T. H.; Sun, Y.; Chai, J. W.; Wang, S. J.; Sun, C. Q. *Surf. Interface Anal.* **2010**, *42*, 878−881.
(54) Chen, L.; Lin, S. D. *Appl. Catal., B* **2011**, *106*, 639−649.
(55) Wen, G.; Xu, Y.; Xu, Z.; Tian, Z. *Catal. Lett.* **2009**, *129*, 250−257.
(56) Lin, W.; Cheng, H.; He, L.; Yu, Y.; Zhao, F. *J. Catal.* **2013**, *303*, 110−116.
(57) De Rogatis, L.; Montini, T.; Lorenzut, B.; Fornasiero, P. *Energy Environ. Sci.* **2008**, *1* (4), 405−512.
(58) Wu, J.; Gao, G.; Li, J.; Sun, P.; Long, X.; Li, F. *Appl. Catal., B* **2017**, *203*, 227−236.
(59) Pan, Y.-T.; Yan, L.; Shao, Y.-T.; Zuo, J.-M.; Yang, H. *Nano Lett.* **2016**, *16*, 7988.
(60) Shan, J.; Zhang, S.; Choksi, T.; Nguyen, L.; Bonifacio, C. S.; Li, Y.; Zhu, W.; Tang, Y.; Zhang, Y.; Yang, J. C.; Greeley, J.; Frenkel, A. I.; Tao, F. *ACS Catal.* **2017**, *7*, 191−204.
(61) Tao, F.; Grass, M. E.; Zhang, Y.; Butcher, D. R.; Renzas, J. R.; Liu, Z.; Chung, J. Y.; Mun, B. S.; Salmeron, M.; Somorjai, G. A. *Science* **2008**, *322*, 932−934.
(62) Yang, Y.; Ma, J.; Jia, X.; Du, Z.; Duan, Y.; Xu, J. *RSC Adv.* **2016**, *6*, 51221−51228.
(63) Gong, W.; Chen, C.; Zhang, H.; Zhang, Y.; Zhang, Y.; Wang, G.; Zhao, H. *J. Mol. Catal. A: Chem.* **2017**, *429*, 51−59.
(64) Kyriakou, G.; Boucher, M. B.; Jewell, A. D.; Lewis, E. a; Lawton, T. J.; Baber, A. E.; Tierney, H. L.; Flytzani-stephanopoulos, M.; Sykes, E. C. H. *Science* **2012**, *335*, 1209−1212.
(65) Dong, F.; Ding, G.; Zheng, H.; Xiang, X.; Chen, L.; Zhu, Y.; Li, Y. *Catal. Sci. Technol.* **2016**, *6*, 767−779.
(66) O'Neill, B. J.; Jackson, D. H. K.; Crisci, A. J.; Farberow, C. A.; Shi, F.; Alba-Rubio, A. C.; Lu, J.; Dietrich, P. J.; Gu, X.; Marshall, C. L.; Stair, P. C.; Elam, J. W.; Miller, J. T.; Ribeiro, F. H.; Voyles, P. M.; Greeley, J.; Mavrikakis, M.; Scott, S. L.; Kuech, T. F.; Dumesic, J. A. *Angew. Chem., Int. Ed.* **2013**, *52*, 13808−13812.
(67) O'Neill, B. J.; Miller, J. T.; Dietrich, P. J.; Sollberger, F. G.; Ribeiro, F. H.; Dumesic, J. A. *ChemCatChem* **2014**, *6*, 2493−2496.
(68) O'Neill, B. J.; Sener, C.; Jackson, D. H. K.; Kuech, T. F.; Dumesic, J. A. *ChemSusChem* **2014**, *7*, 3247−3251.
(69) Biswas, P.; Lin, J. H.; Kang, J.; Guliants, V. V. *Appl. Catal., A* **2014**, *475*, 379−385.
(70) Ding, F.; Zhang, Y.; Yuan, G.; Wang, K.; Dragutan, I.; Dragutan, V.; Cui, Y.; Wu, J. *J. Nanomater.* **2015**, *2015*, 1−6.
(71) Perret, N.; Grigoropoulos, A.; Zanella, M.; Manning, T. D.; Claridge, J. B.; Rosseinsky, M. J. *ChemSusChem* **2016**, *9*, 521−531.
(72) Liu, J.; Lucci, F. R.; Yang, M.; Lee, S.; Marcinkowski, M. D.; Therrien, A. J.; Williams, C. T.; Sykes, E. C. H.; Flytzani-Stephanopoulos, M. *J. Am. Chem. Soc.* **2016**, *138*, 6396−6399.
(73) Pei, G. X.; Liu, X. Y.; Wang, A.; Lee, A. F.; Isaacs, M. A.; Li, L.; Pan, X.; Yang, X.; Wang, X.; Tai, Z.; Wilson, K.; Zhang, T. *ACS Catal.* **2015**, *5*, 3717−3725.
(74) Van Cleve, T.; Moniri, S.; Belok, G.; More, K. L.; Linic, S. *ACS Catal.* **2017**, *7*, 17−24.
(75) Greeley, J.; Mavrikakis, M. *Nat. Mater.* **2004**, *3*, 810−815.
(76) Nelson, R. C.; Baek, B.; Ruiz, P.; Goundie, B.; Brooks, A.; Wheeler, M. C.; Frederick, B. G.; Grabow, L. C.; Austin, R. N. *ACS Catal.* **2015**, *5*, 6509−6523.

DOI: 10.1021/acscatal.7b01095
ACS Catal. 2017, 7, 4070−4082

(77) Omotoso, T.; Boonyasuwat, S.; Crossley, S. P. *Green Chem.* **2014**, *16*, 645−652.
(78) Matsubu, J. C.; Zhang, S.; Derita, L.; Marinkovic, N. S.; Chen, J. G.; Graham, G. W.; Pan, X.; Christopher, P. *Nat. Chem.* **2017**, *9*, 120−127.
(79) Tauster, S. J. *Acc. Chem. Res.* **1987**, *20*, 389−394.
(80) Tauster, S. J.; Fung, S. C.; Garten, R. L. *J. Am. Chem. Soc.* **1978**, *100*, 170−175.
(81) Carrero, A.; Calles, J. A.; Vizcaíno, A. J. *Appl. Catal., A* **2007**, *327*, 82−94.
(82) Huang, T.; Yu, T.; Jhao, S. *Ind. Eng. Chem. Res.* **2006**, *45*, 150−156.
(83) Marino, J.; Cerrella, E.; Duhalde, S.; Jobbagy, M.; Laborde, M. A. *Int. J. Hydrogen Energy* **1998**, *23*, 1095−1101.
(84) Sinfelt, J. H. *Acc. Chem. Res.* **1977**, *10*, 15−20.
(85) Uchiyama, S.; Ohbayashi, Y.; Hayasaka, T.; Kawata, N. *Appl. Catal.* **1988**, *42*, 143−152.
(86) Swift, H. E.; Lutinski, F. E.; Kehl, W. L. *J. Phys. Chem.* **1965**, *69*, 3268−3274.
(87) Wang, F.; Li, Y.; Cai, W.; Zhan, E.; Mu, X.; Shen, W. *Catal. Today* **2009**, *146*, 31−36.
(88) Wang, H.; Baker, R. T. K. *J. Phys. Chem. B* **2004**, *108*, 20273−20277.
(89) Wolfbeisser, A.; Klötzer, B.; Mayr, L.; Rameshan, R.; Zemlyanov, D.; Bernardi, J.; Föttinger, K.; Rupprechter, G. *Catal. Sci. Technol.* **2015**, *5*, 967−978.
(90) Bonet, F.; Grugeon, S.; Dupont, L.; Herrera Urbina, R.; Guery, C.; Tarascon, J. M. *J. Solid State Chem.* **2003**, *172*, 111−115.
(91) Brongersma, H. H.; Sparnaay, M. J.; Buck, T. M. *Surf. Sci.* **1978**, *71*, 657−678.
(92) Egelhoff, W. F. *Phys. Rev. Lett.* **1983**, *50*, 587−590.
(93) Sinfelt, J. H.; Carter, J. L.; Yates, D. J. C. *J. Catal.* **1972**, *24*, 283−296.
(94) Wandelt, K.; Brundle, C. R. *Phys. Rev. Lett.* **1981**, *46*, 1529−1532.
(95) Webber, P. R.; Rojas, C. E.; Dobson, P. J.; Chadwick, D. *Surf. Sci.* **1981**, *105*, 20−40.
(96) Ferrando, R.; Jellinek, J.; Johnston, R. L. *Chem. Rev.* **2008**, *108*, 845−910.
(97) Mariño, F.; Baronetti, G.; Jobbagy, M.; Laborde, M. *Appl. Catal., A* **2003**, *238*, 41−54.
(98) Studt, F.; Abild-pedersen, F.; Wu, Q.; Jensen, A. D.; Temel, B.; Grunwaldt, J.; Nørskov, J. K. *J. Catal.* **2012**, *293*, 51−60.
(99) Ranga Rao, G.; Meher, S. K.; Mishra, B. G.; Charan, P. H. K. *Catal. Today* **2012**, *198*, 140−147.
(100) Ungureanu, A.; Dragoi, B.; Chirieac, A.; Royer, S.; Duprez, D.; Dumitriu, E. *J. Mater. Chem.* **2011**, *21*, 12529−12541.
(101) Xiong, K.; Wan, W.; Chen, J. G. *Surf. Sci.* **2016**, *652*, 91−97.

DOI: 10.1021/acscatal.7b01095
ACS Catal. 2017, 7, 4070−4082